

**Room temperature co-precipitation synthesis of magnetite nanoparticles in large pH window with different bases.**

*Maria Cristina Mascolo<sup>a c</sup> Yongbing Pei<sup>a b</sup>, Terry A. Ring<sup>a\*</sup>*

<sup>a</sup> Department of Chemical Engineering, University of Utah, Salt Lake City, 84112, USA

<sup>b</sup> School of Chemistry and Chemical Engineering, South China University of China, Guangzhou, 510640, China

<sup>c</sup> Laboratorio Materiali del Dipartimento di Meccanica, Strutture, Ambiente e Territorio, Università di Cassino, Via G. Di Biasio 43, 3043 Cassino (FR), Italy

*Corresponding author:* Prof. Terry A. Ring, Department of Chemical Engineering, University of Utah, Salt Lake City, UT 84112 USA.

E-mail: t.ring@utah.edu

**Abstract:**

Magnetite nanoparticles ( $\text{Fe}_3\text{O}_4$ ) were synthesized using one pot co-precipitation reaction at room temperature in the presence either of stoichiometric or of an excess of different bases such as NaOH, KOH or  $(\text{C}_2\text{H}_5)_4\text{NOH}$ . A slow or fast addition of the precipitating alkaline solution into reaction solution, containing ferric and ferrous ions in the molar ratio 2:1, were adopted. The magnetite nanoparticles show characteristics of superparamagnetism at room temperature. The saturation magnetization ( $M_s$ ) decreases from 75.3 to 52.3 emu/g and magnetite particle size decreases from 11.5 to 6.4 nm.

The aggregation of the primary particles of magnetite, responsible of the formation of a mesoporous structure, is affected by the pH, the nature of alkali and by the slow or fast addition of alkaline solution.

**Keywords:** magnetite nanoparticles, co-precipitation, room temperature, superpagnetism, aggregation, mesoporous structure.

## 1. Introduction

Magnetite is a ferrimagnetic material with a cubic inverse spinel structure. A normal spinel has the formula  $AB_2O_4$  with divalent A atoms in the tetrahedral sites and both trivalent B atoms in the octahedral sites. Inverse spinels have B atoms in the tetrahedral sites and both A and B atoms in the octahedral sites - the ferric ion (B atom) occupies the tetrahedral site and both the ferric and ferrous atoms randomly occupy the octahedral sites. Magnetite has been widely investigated for its potential applications in many areas such as biomedical [1-3], target drug delivery [4], tumor and cancer diagnosis and treatment [5], and as a magnetic resonance imaging (MRI) contrasting agent [6, 7]. All of these medical applications require that the magnetite nanoparticles are superparamagnetic with sizes smaller than 20 nm [8]. Magnetite adsorbs oxygen to form maghemite which in turn loses its susceptibility with time [9]. On the other hand, the nanosized particles form less stable systems from the colloidal point of view determining their aggregation. In the case of magnetic fluids, to prevent aggregation of the primary particles during thermal motion, the coating of the particle surface is essential. The coated nanoparticles can form stable colloidal dispersion in a wide pH range [10, 11]. In addition the adsorption layer can also enhance resistance against chemical transformation of magnetite-maghemite solids.

The applications of these nano-materials depend on the preparation method which influences particle size and shape, size distribution, aggregation and surface chemistry of the material. The magnetite nanoparticles can be prepared by various synthetic methods including: ultrasound irradiation [12], sol-gel [13], thermal decomposition [8, 14-18] and co-precipitation [19-25]. Thermal decomposition and co-precipitation are the two

methods most commonly used. The thermal decomposition route relies on the pyrolysis of organic compounds of iron  $\text{Fe}(\text{CO})_5$  [14-15] and  $\text{Fe}(\text{acac})_3$  [8, 16-18] are the most commonly used precursors. However,  $\text{Fe}(\text{CO})_5$  and  $\text{Fe}(\text{acac})_3$  are toxic and may limit the application of magnetite for medical applications. Recently, using  $[\text{Fe}(\text{CON}_2\text{H}_4)_6](\text{NO}_3)_3$  [26] as precursor, a one pot synthesis of magnetite was reported, which has broadened the precursor types for thermal decomposition. Co-precipitations based on the hydrolysis of a mixture of ferrous and ferric ions, are used to fix the A to B molar ratio in the inverse spinel structure. Generally the reaction is performed under an inert ( $\text{N}_2$  or Ar) atmosphere using degassed solutions to avoid uncontrollable oxidizing of  $\text{Fe}^{2+}$  to  $\text{Fe}^{3+}$  [24]. In this method, ferrous and ferric ions are generally precipitated in alkaline solutions, such as ammonium hydroxide, potassium hydroxide or sodium hydroxide. In most cases the solution is heated to 70-80 ° C [25], or higher temperatures. The effects of mixing methods [20], stirring rate [27], digestion time [28], initial pH [29] and the presence or absence of a magnetic field [19, 30] during precipitation on particle size, morphology and resulting magnetic properties were also discussed. Co-precipitation methods that have been used by others show various precipitation conditions. For example, only  $\text{Fe}^{2+}$  was used for precipitation. Then  $\text{H}_2\text{O}_2$  [19-20] or  $\text{NaNO}_2$  [21] was used to partially oxidize ferrous to ferric ion in the precipitated product. Or only  $\text{Fe}^{3+}$  was used for precipitation. Then  $\text{Na}_2\text{SO}_3$  [22] was used to partially reduce ferric to ferrous ion in the precipitation product. Some co-precipitation methods are in the presence of polymers [23] including: polyvinyl alcohol (PVA) and dextran to prevent aggregation of the nanoparticles. All these co-precipitation methods are comparatively complex and require strict control of precipitation conditions.

Here, recent work is reported that clarifies the chemistry of the synthesis of magnetite using the co-precipitation method. Magnetite nanoparticles are prepared in a simple, one-pot, room-temperature reaction using  $\text{FeCl}_3 \cdot 6\text{H}_2\text{O}$  and  $\text{FeCl}_2 \cdot 4\text{H}_2\text{O}$  as raw materials. A stoichiometric mixture of ferrous and ferric ions is reacted with alkaline solutions. Two series of samples have been prepared: the first one by slow addition, 1.0 mL/min of the alkaline solution into 100 mL reaction solution, whereas the second series was obtained by a fast addition of the alkaline solution to the reaction solution. The different alkaline solutions contained stoichiometric or excesses of NaOH, KOH or  $(\text{C}_2\text{H}_5)_4\text{NOH}$ , respectively. The main advantage of this method is its simplicity and no need for high temperatures during precipitation nor heat treatments/calcination after precipitation nor subsequent oxidation or reduction reactions to develop the magnetite (oxide) phase from the precipitated hydroxide phase.

## **2. Analysis of Magnetite Synthesis Routes**

Many of the co-precipitation routes require elevated temperatures for magnetite synthesis. To evaluate the effects of temperature on the synthesis of magnetite, OLI Systems LabAnalyzer software was used. In this software, solution equilibria account for all solution complexes and the solubility of various solids, simultaneously. Table 1 gives a list of solution complexes and solids phases. The solutions are non-ideal with activity coefficients being calculated for each species in solution using extended Debye-Huckel theory. The solution conditions used for this analysis are 0.1 mol/L  $\text{FeCl}_3$ , 0.05 mol/L  $\text{FeCl}_2$  in deionized water and various NaOH concentrations to give various pH values at equilibrium. Solution equilibria are calculated for different temperatures from 0 to 100 °C at one atmosphere total pressure. The results are shown in figure 1(a) and 1(b).

Figure 1(a) shows the solid concentration in equilibrium with the solution as a function of temperature for various pH conditions which are equivalent to various amounts of NaOH added during co-precipitation. Here we see that a stoichiometric ratio of  $\text{Fe}^{3+}$  to  $\text{Fe}^{2+}$  equal to 2:1 in the solid phase is best achieved at room temperatures which give the largest window of pH values, from 10.0 to 13.0, where a near perfect 2:1 stoichiometric solid may be produced. At higher temperatures 70-80 °C, the product precipitated from a 2:1 stoichiometric solution is not stoichiometric except in a narrow pH window. The dominant solids of  $\text{Fe}^{3+}$  and  $\text{Fe}^{2+}$  ions start to deviate from 0.1 mol/L and 0.05 mol/L at a pH values greater than 12.0 or 13.0, depending upon temperature. Figure 1(b) shows the solids ratio of  $\text{Fe}(\text{OH})_3$  to  $\text{Fe}(\text{OH})_2$ . We see that at 20-30 °C, this ratio keeps perfect close to 2.0 in the pH window from 10.0 to 13.0. At higher temperatures 70-80 °C, a 2:1 stoichiometric solution only produces a 2:1 stoichiometric solid at pH values less than 12.0, and this ratio starts to deviate from 2.0 at pH values greater than 12.0. This is contrary to the method of increasing pH ( $\text{OH}^-$  concentration) to high values in order to completely precipitate the iron species as hydroxides used by experimentalists. At low temperatures, the window closes due to the solubility of  $\text{Fe}^{2+}$  ion solubility at low pH. At high temperature, the window closes due to the solubility of both ferrous  $[\text{Fe}(\text{OH})_4]^{2-}$  and ferric  $[\text{Fe}(\text{OH})_4]^-$  ions solubility to different degrees at high pH. As a result of this analysis the following room temperature experimental method was developed.

### **3. Experimental**

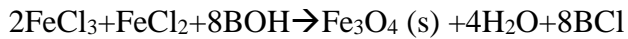
#### *3.1. Chemicals and Equipment*

The chemicals used,  $\text{FeCl}_3 \cdot 6\text{H}_2\text{O}$ ,  $\text{FeCl}_2 \cdot 4\text{H}_2\text{O}$ , NaOH, KOH,  $(\text{C}_2\text{H}_5)_4\text{NOH}$ , were purchased from Sigma-Aldrich and used without further purification. To avoid the

formation of both maghemite,  $\gamma\text{-Fe}_2\text{O}_3$ , and hematite,  $\alpha\text{-Fe}_2\text{O}_3$ , all the syntheses were performed under oxygen free conditions. To this end, deionized water was boiled to remove dissolved oxygen and stored in a sealed glass container before use. Solutions were made with degassed deionized water. The reactions were performed under a nitrogen atmosphere using high purity nitrogen from Air Products. Two series of samples have been prepared: the first one by slow addition, 1.0 mL/min, of the alkaline solution into the reaction solution, whereas the second series was obtained by a fast addition of the alkaline solution to the reaction solution. A precision pump operating at a flow rate of  $1.0\pm 0.1$  ml/min was used for the addition of reactants to the reaction vessel.

### 3.2 Synthesis

$\text{Fe}_3\text{O}_4$  was synthesized in alkaline conditions using different bases BOH, with B =  $\text{Na}^+$ ,  $\text{K}^+$  or  $(\text{C}_2\text{H}_5)_4\text{N}^+$ , to complete the following overall reaction:



To investigate the effect of pH value on properties of magnetite nanoparticles, the experiments were conducted at various BOH amounts. During the reaction, the reaction flask was equipped with a pH meter to measure the final pH value. The experimental parameters for the synthesis of magnetite nano-particles are summarized in Table 2. The coprecipitation of iron ions has been performed either with stoichiometric or with excesses of BOH solution adopting a slow (S) or a fast (F) addition of the precipitating alkaline solution.

In a typical experiment (S1 sample), 0.01 mol  $\text{FeCl}_2 \cdot 4\text{H}_2\text{O}$  and 0.02 mol  $\text{FeCl}_3 \cdot 6\text{H}_2\text{O}$  were dissolved with 100 ml degassed deionized water and added into a 250 ml three neck flask which was immersed in a room temperature (25 °C) water bath. 0.08 mol NaOH was dissolved in 100 ml degassed deionized water. For slow addition the NaOH solution was then added to the reaction flask using a pump operating at approximately  $1.0 \pm 0.1 \text{ ml min}^{-1}$ . The reaction solution was mechanically stirred at 500 rpm while nitrogen gas flowed into the flask. After charging of the reactor with NaOH was completed, stirring continued for 3 hours after which the final pH was recorded. After the reaction was completed, the magnetite particles were isolated by using a permanent magnet. The solution was decanted in this way allowing the particles to be washed with degassed deionized water. This procedure was repeated six times and then the particles were isolated by a permanent magnet and dried in a vacuum desiccator.

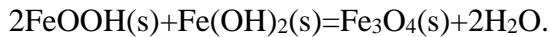
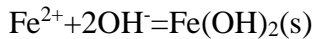
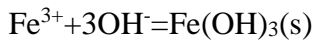
### *3.3 Characterization*

The crystal structure of the synthesized particles was characterized by X-ray diffraction (XRD) measurement (PANalytical B.V. Netherlands) using  $\text{Cu-K}_\alpha$  ( $\lambda = 0.154060 \text{ nm}$ ) radiation (step time 10 s; step size  $0.05^\circ$ ;  $2\theta = 5\text{-}95^\circ$ ). Specific surface area was measured by BET method and the pore sizes distribution of the powders by the adsorption-desorption isotherm utilizing nitrogen as adsorbate after drying at 80 °C for 12 h (Gemini 2375, Micromeritics, USA). The magnetite nanoparticle morphology was investigated by scanning electron microscopy (SEM) (FEI Quanta 600 FEG, USA) with a field emission electron gun operated at 25 kV and a magnification of 5000X. Transmission electron microscopy (TEM) study was carried out on a electron microscopy instrument (FEI Tecnai G12 Spirit Twin, USA). The powders for TEM were dispersed in

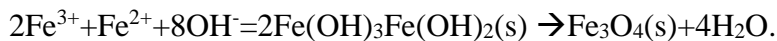
ethanol; the suspension was then dropped on carbon-copper grids. The magnetic properties of the particles were measured with a Physical Properties Measurement System magnetometer at 298 K (Quantum Design, USA). The magnetization measurement was taken from -10 kOe to 10 kOe field. From the magnetization versus applied field curve, the saturation magnetization (Ms) was measured.

#### 4. Results and Discussion

The co-precipitation method using ferrous and ferric ions reacting in alkaline conditions has been extensively investigated [24, 27-30], and the following reactions are proposed for the mechanism of magnetite formation:



Giving an overall reaction:



First, the ferric and ferrous hydroxides are precipitated. These reactions are very fast. Second, the ferric hydroxide decomposes to FeOOH due to the low water activity of the resulting NaCl solution in a slower reaction. Finally, a solid state reaction between FeOOH and Fe(OH)<sub>2</sub> takes place due to the low water activity of the solution, which produces magnetite. This solid state reaction takes place between 10-30 minutes at room temperature. The overall reaction mechanism is a dynamic equilibrium equation in which

the concentration and size of Fe<sub>3</sub>O<sub>4</sub> nanoparticles are influenced by [Fe<sup>3+</sup>], [Fe<sup>2+</sup>] and [OH<sup>-</sup>] as well as the water activity of the solution. We design ferric to ferrous molar ratio as 2:1, which is the exact stoichiometry for magnetite, in order to produce high purity magnetite nanoparticles. The final [OH<sup>-</sup>] concentration, which is related to the pH and base amount, is known to control the nucleation and growth of the magnetite nanoparticles and can influence the magnetite properties, e.g. particle size and saturation magnetization (Ms). In this study the room temperature synthesis of magnetite, obtained at various pH values by varying the nature of the base and its amount is reported.

#### *4.1 XRD pattern*

Figure 2 shows the XRD patterns of magnetite particles synthesized by slow addition at various NaOH amounts and pH values. The largest diffraction peaks occur at  $2\theta = 30.1^\circ$ ,  $35.4^\circ$ ,  $43.1^\circ$ ,  $53.4^\circ$ ,  $57.0^\circ$ ,  $62.5^\circ$ , which can be indexed to the [2 2 0], [3 1 1], [4 0 0], [4 2 2], [5 1 1], [4 4 0] planes of spinel structure for magnetite respectively. When compared with the structure of Fe<sub>3</sub>O<sub>4</sub> (JCPDS file, No. 00-011-0614), the diffraction pattern peaks correspond well to magnetite Fe<sub>3</sub>O<sub>4</sub>. The products synthesized by fast addition also show XRD patterns typical of magnetite particles.

An estimation of the magnetite nanoparticles size can be performed from Scherrer formula:

$$D = \frac{K\lambda}{B \cos \theta}$$

where  $\lambda$  is the X-ray wavelength (0.15406 nm), B is the full width at half maximum (FWHM),  $\theta$  is the corresponding Bragg angle, and K is the shape parameter which is 0.89 for magnetite. Taking the highest intensity peak, namely the [3 1 1] plane, at  $2\theta = 35.4^\circ$  and half maximum intensity width of the peak after accounting for instrument broadening,

the calculated particle sizes are 11.5 nm, 11.2 nm, 11.0 nm, 10.9 nm and 10.7 nm for samples S1, S2, S3, S4 and S5, respectively ( 2<sup>nd</sup> column of Table 3). As NaOH amount and pH increases, the nanoparticle size decreases albeit a small amount. At higher pH, supersaturation during co-precipitation is higher promoting nucleation over growth thus giving smaller particle sizes. By using the co-precipitation method over this wide range of pH values at room temperature, it is easy to prepare magnetite nanoparticles with an approximate size of 11.0 nm.

Note that in the XRD patterns the peak positions shift slightly toward larger  $2\theta$  values with increasing pH. Taking the [311] peak as a representative, figure 3 shows a magnified representation of all XRD patterns. Figure 3 clearly shows the peaks shift, indicating that the lattice parameter contracts as the particle size decreases. This phenomenon has also been observed and reported in previous works [28, 31].

The fast addition of the stoichiometric or of the more concentrated NaOH solution to the reaction solution determines the formation of magnetite nanoparticles smaller in sizes, 10.2 and 8.2 nm for F1<sub>Na</sub> and F5<sub>Na</sub> samples, respectively in comparison to those of the corresponding magnetite obtained by slow addition of the base. The nature of the precipitating base also affects the particle sizes. Smaller magnetite nanoparticles of 7.1 and 6.5 nm result for F3<sub>K</sub> and F3<sub>TEA</sub> samples synthesized by fast addition of KOH and TEAOH, respectively. The sample \*F3<sub>TEA</sub>, synthesized with a reverse modality by fast addition of ferrous and ferric ions into TEAOH solution shows magnetite nanoparticles of 6.4 nm, a size very similar to that of the F3<sub>TEA</sub> sample synthesized by fast addition of TEAOH solution into the iron chlorides-containing solution.

#### *4.2 BET measurement*

Table 3 shows also the specific surface area measured by BET method (4<sup>th</sup> column of Table 3) and saturation magnetization (Ms) of the magnetite nanoparticles (7<sup>th</sup> column) synthesized at various conditions. The saturation magnetization is discussed later. Here, the listed particle size is calculated either from XRD (2<sup>nd</sup> column) and from BET measurement (3<sup>rd</sup> column) adopting the particles diameter, D, given by:

$$D = \frac{6}{S_{sp} \rho_a}$$

where  $S_{sp}$  is the specific surface area of the sample and  $\rho_a$  is the density 5.18 g/cm<sup>3</sup>. We can see that, when pH increases, the specific surface area increases and particle size decreases. The sizes calculated from BET measurements for samples S1, S2, S3, S4 and S5 respectively, compared with the size from XRD, result approximately 10 % slightly larger. Such difference in size for the magnetite samples synthesized by fast addition of the base changes from 15 % for F1<sub>Na</sub> sample to 1.5 % for \*F3<sub>TEA</sub> sample, respectively. These detected differences can be explained with the agglomeration of the primary particles of magnetite giving lower surface area and, consequently, an apparently larger particle size. Such agglomeration has been evaluated determining the interface area among the primary particles of magnetite adopting the formula.  $(S_{XRD} - S_{BET})/2$ , where  $S_{XRD}$  is the surface area calculated from crystal size measured with Sherrer formula, whereas  $S_{BET}$  is the surface area determined with the BET method. With the exception of the \*F3<sub>TEA</sub> sample, an interface area approximately 5 m<sup>2</sup>/g results for the remaining magnetite samples. The agglomeration of the primary nanosized particles of magnetite is confirmed by the N<sub>2</sub> adsorption-desorption isotherms shown in Fig.4 for the samples S1 S5, F1<sub>Na</sub> and F5<sub>Na</sub>, respectively. With the exception of the \*F3<sub>TEA</sub> sample, each product is

characterized, in fact, by a clear hysteresis loop which is typical of mesoporous products as a consequence of the agglomeration. The corresponding BJH pore size distribution determined from the desorption branch isotherm are shown in Fig.5. A pore size distribution with pores changing in the mesopore range results for all the samples. The maximum of the pore size is affected by the particle size of magnetite. Smaller particle size of magnetite, lower the maximum of the pore size results. The fast addition with an excess of the NaOH solution gives a magnetite product with the maximum shifted to smaller values of mesopores. It is also evident that broader pore size distribution characterizes the products synthesized by slow addition of the basic solution in comparison to that of the products obtained by fast addition of the precipitating base.

#### *4.3 SEM and TEM images*

Figure 6 shows SEM images of S3 and S5 samples and TEM images of X and \*F3<sub>TEA</sub> samples, respectively.

SEM images show the particles appears uniform and their primary particles are approximately 11.0 nm in size, indicating that magnetite nanoparticles with uniform size can be synthesized in a large pH window at room temperature. The primary particles of magnetite are more or less aggregates so determining, in the absence of a surfactant, the formation of aggregates with broad range of mesopores as can be seen in the TEM images of Fig. 6c and 6d. The TEM images of \*F3<sub>TEA</sub> in Fig. 6e and 6f, shows single magnetite particles due to the very poor aggregation of the primary particles. Such findings justify the different behaviour of this sample in terms of stability suspension of

magnetic particles in the liquid medium. The \*F3<sub>TEA</sub> sample results a perfect colloidal suspension due to the absence of any particle sedimentation after several months of aging, whereas for all the other samples the sedimentation of aggregates results in more or less short times for sedimentation. This behaviour can be related to two concomitant effects of the basic solution of the TEAOH. The magnetic particles synthesized in the presence of TEAOH are very small in size so that their thermal energy is large enough to overcome the energy of the magnetic interactions among the magnetite particles (32). The OH<sup>-</sup> ions of the basic TEAOH-containing solution are adsorbed on the magnetite particles determining a negative charge on each particle. As a surfactant, the positively-charged tetraethylammonium ions forms a shell around each magnetite particle so raising the energy required for the particles to agglomerate, stabilizing the corresponding colloidal suspension. For the F3<sub>TEA</sub> sample, obtained by fast addition of the TEAOH solution into iron chlorides-containing solution, the sedimentation of magnetite particles occurs. Such a difference might be related to the more basic medium in the first step of the reaction when iron chlorides are fastly added to TEAOH.

#### *4.4 Magnetic properties*

The magnetization curve for the synthesized magnetite nanoparticles reported in Figure 7 does not show any hysteresis behavior for any of the samples and exhibits immeasurable values of coercivity field and remnant magnetization. This confirms that the synthesized particles exhibit superparamagnetic properties at room temperature. This is in good agreement with a previous studies that magnetite nanoparticles exhibit superparamagnetic properties when they are smaller than critical size the magnetic domain size (33).

Table 3 shows the saturation magnetization ( $M_s$ ) of all the synthesized samples. We can see that  $M_s$  values decrease as the magnetite particles size decrease. This is due to the size effect which has been reported previously [26, 28-29, 31].

## 5. Conclusions

A simplified co-precipitation method has been utilized to synthesize magnetite nanoparticles exhibiting superparamagnetic behaviour. They were formed by a one pot co-precipitation reaction in a large pH window (10.0-13.0) at room temperature. Magnetite nanoparticles, whose average particle size is about 11.0 nm, were synthesized by slow addition of NaOH solutions into solutions of ferric and ferrous ions in a 2:1 ratio. Smaller particle sizes of magnetite are obtained by fast addition of the basic solution to the solution of mixed  $Fe^{+2}$  and  $Fe^{+3}$  ions. A further size reduction of magnetite can be determined by the nature of the precipitating base. The decrease of the particle size of magnetite is, in fact, in accordance with the following sequence:  $NaOH > KOH > (C_2H_5)_4NOH$ . The magnetite with the lowest particle size of 6.4 nm was synthesized by fast addition of iron ions-containing solution into the solution characterized by an excess of TEAOH. The small particle size of this product and the negligible agglomeration of the primary particles favour the formation, in a single step, of a very stable colloidal suspension.

The resulting magnetite nanoparticles exhibit superparamagnetic properties depending on the particle size. Lower the particle size of magnetite, lower is the saturation magnetization ( $M_s$ ). For the particle size of magnetite changing between 6.4÷11.5 nm,  $M_s$  changes from 52.3 emu/g to 75.3 emu/g.

The detected agglomeration among the nanoparticles of all the remaining samples justifies the formation of mesopores whose average size is affected by the primary particles of magnetite. Mesopores larger in size resulted, in fact, with bigger primary particles, whereas mesopores smaller in size with smaller primary particles.

The synthesized magnetite nanoparticles with mesoporous structure appears very promising for biomedical applications. It is well known that because of the low drug or enzyme loading on the conventional magnetite nanoparticles, the magnetic material are often incorporated into mesoporous materials to form hybrid support with consequent reduction of MS. The synthesized products, being combinations of mesoporous properties with magnetic property, appear of interest for biomedical applications.

### **Acknowledgments**

We appreciate much to the financial support from the Chinese Scholarship Council which has provided support for an author to perform this research at the University of Utah. OLI Systems, Inc is thanked for use of the LabAnalyzer™ software. Joseph G. Bolke, Alex Hogan and Amber C. McConnell from the Departments of Material Science (Nanolab) and Chemistry at the University of Utah are thanked for assistance with XRD, SEM and magnetic measurements. Thanks are also due to LaMEST of ICTP/IMCB of CNR, Pozzuoli-Italy for TEM measurements.

### **Reference**

- [1]. K. Nishio, M. Ikeda, N. Gokon, S. Tsubouchi, H. Narimatsu, Y. Mochizuki, S. Sakamoto, A. Sandhu, M. Abe, H. Handa. *J. Magn. Magn. Mater.* 310 (2007) 2408–2410.
- [2]. A.K. Gupta and M. Gupta, *Biomaterials*, 26 (2005), 3995-4021.
- [3]. Y. W. Jun, J. H. Lee, J. Cheon, *Angew. Chem., Int. Ed.*, 47 (2008), 5122-5135.
- [4]. J.B.A. Sudimack, R.J. Lee. *Adv. Drug Delivery Rev.* 41(2000)147-162.
- [5]. A. Jordan, R. Scholz, K. Maier-hauff, M. Johannsen, P. Wust, J. Nadobny, H. Schirra, H. Schmidt, S. Deger, S. Loening, W. Lanksch, R. Felix. *J. Magn. Magn. Mater.* 225(2001) 118-126.
- [6]. F. Hu, L. Wei, Z. Zhou, Y. Ran, Z. Li, M. Gao. *Adv. Mater.* 18(2006) 2553-2556.
- [7]. H. Song, J. Choi, Y. Huh, S. Kim, Y. Jun, J. Suh, J. Cheon. *J. Am. Chem. Soc.* 127(2005)9992-9993.
- [8]. S. Sun, H. Zeng. *J. AM. Chem. Soc.* 124(2002)8204-8205.
- [9]. R. Dronskowski, *Advanced Functional Materials*, 11, 1 (2001), 27-29.
- [10]. P. Tartaj, M. P. Morales, T. Gonzales-Carreno, S. Veintemillas-Verdaguer, C. J. Serna, *J. of Magnetism and Magnetic Materials* 290 (2005), 28-34;
- [11]. Petri-Fink, M. Chastellain, L. Juillerat-Jeanneret, A. Ferrari, H. Hofmann, *Biomaterials*, 26,15 (2005), 2685-2694. ]
- [12]. B.M. Teo, F. Chen, T.A. Hatton, F. Grieser, M. Ashokkumar. *Langmuir.* 25(2009)2593-2595.
- [13]. A.S. Teja, P. Koh. *Prog Cryst. Growth Charact. Mater.* 55(2009)22-45.
- [14]. S. Peng, C. Wang, J. Xie, S. Sun. *J. Am. Chem. Soc.* 128(2006)10676-10677.
- [15]. J. Ge, Y. Hu, M. Biasini, C. Dong, J. Guo, W.P. Beyermann, Y. Yin. *Chem. Eur. J.* 13(2007)7153-7161.

- [16]. X. Lu, M. Niu, R. Qiao, M. Gao. *J. Phys. Chem. B.* 112(2008)14390-14394.
- [17]. Z. Li, H. Chen, H. Bao, M. Gao. *Chem. Mater.* 16(2004)1391-1393.
- [18]. J.M. Vargas, R.D. Zysler. *Nanotech.* 16(2005)1474-1476.
- [19]. D. Hu, Y. Wang, Q. Song. *Particuology.* 7 (2009)363–367.
- [20]. Y. Mizukoshi, T. Shuto, N. Masahashi, S. Tanabe. *Ultrason. Sonochem.* 16(2009)525–531.
- [21]. I. Nedkov, T. Merodiiska, L. Slavov, R.E. Vandenberghe, Y. Kusano, J. Takada. *J. Magn. Mater.* 300(2006)358–367
- [22]. S. Qu, H. Yang, D. Ren, S. Kan, G. Zou, D. Li, M. Li. *J. Colloid Interface Sci.* 215(1999)190–192.
- [23]. H. Pardoe, W. Chua-anusorn, T.G.S. Pierre, J. Dobson. *J. Magn. Mater.* 225(2001)41-46.
- [24]. A. Bandhu, S. Mukherjee, S. Acharya, S. Modak, S.K. Brahma, D. Das, P.K. Chakrabarti. *Solid State Commun.* 149(2009)1790-1794.
- [25]. T. Ozkaya, M.S. Toprak, A. Baykal, H. Kavaz, Y. Koseoglu, B. Aktas. *J. Alloys Compd.* 472(2009)18-23.
- [26]. S. Zhao, S. Asuha. *Powder Technol.* 197(2010)295-297.
- [27]. R. Valenzuela, M.C. Fuentes, C. Parra, J. Baeza, N. Duran, S.K. Sharma, M. Knobel, J. Freer. *J. Alloys Compd.* 488(2009)227–231.
- [28]. G. Gnanaprakash, J. Philip, T. Jayakumar, B. Raj. *J. Phys. Chem. B.* 111(2007)7978-7986.
- [29]. G. Gnanaprakash, S. Mahadevan, T. Jayakumar, P. Kalyanasundaram, J. Philip, B. Raj. *Mater. Chem. Phys.* 103(2007)168-175.

- [30]. F. Vereda, J. Vicente, R. Hidalgo-Alvarez. *Langmuir*. 23(2007)3581-3589.
- [31]. J.Y. Park, D. Patel, E.S. Choi, M.J. Baek, Y. Chang, T.J. Kim, G.H. Lee. *Colloids Surf., A*. 367(2010)41-46.
- [32]. J.P. Jolivet, R. Massart, J.M. Fruchart, *Nouv. J. Chim.* 1983,7,325
- [33]. D.J. Dunlop. *J. Geophys. Res.* 78(1973)1780-1793.

## List of Tables

Table 1. Solution Complexes and Solid Phases in Equilibria Calculations.

Table 2. Experimental parameters.

Table 3. Properties of the magnetite nanoparticles synthesized at various amounts with different bases-containing solutions

## List of Figures

Figure 1(a). Dominant Solids ( $\text{Fe}(\text{OH})_2$  and  $\text{Fe}(\text{OH})_3$ ) concentration [mol/L] as a function of temperature at various pH values.

Figure 1(b). Dominant solids ratio of  $\text{Fe}(\text{OH})_3$  to  $\text{Fe}(\text{OH})_2$  at room temperature (20-30 °C) and high temperature (70-80 °C) at various pH values.

Figure 2. X-ray diffraction of magnetite nanoparticles synthesized at various NaOH amounts.

Figure 3. [3 1 1] peaks of the magnetite nanoparticles in expanded  $2\theta$  scale.

Figure 4.  $\text{N}_2$  adsorption-desorption isotherms of S1, S5, F1<sub>Na</sub> and F5<sub>Na</sub> samples.

Figure 5. BJH desorption pore size distribution curves for S1, S5, F1<sub>Na</sub> and F5<sub>Na</sub> samples

Figure 6. SEM images of S4 (a), S5 (b) samples and TEM images of F3<sub>Na</sub> (c, d), F3<sub>TEA</sub> (e, f).

Figure 7. Magnetization curve for S1, S5, F1<sub>Na</sub> and F5<sub>Na</sub> samples

Table 1. Solution Complexes and Solid Phases in Equilibria Calculations.KOH TEAOH ??

Solid Phases	Solution Complex Species		
Fe(OH) <sub>2</sub>	FeCl <sub>2</sub>	OH <sup>-</sup>	[FeCl <sub>2</sub> ] <sup>+</sup>
Fe(OH) <sub>3</sub>	FeCl <sub>3</sub>	Fe <sup>2+</sup>	[Fe(OH) <sub>2</sub> ] <sup>+</sup>
NaCl	HCl	Fe <sup>3+</sup>	[FeCl] <sup>2+</sup>
FeCl <sub>2</sub> ·4H <sub>2</sub> O	Aqueous Fe(OH) <sub>3</sub> and Fe(OH) <sub>2</sub> precipitation precursors	[FeCl] <sup>+</sup>	[Fe(OH)] <sup>2+</sup>
FeCl <sub>2</sub>	Cl <sup>-</sup>	[FeOH] <sup>+</sup>	[FeCl <sub>4</sub> ] <sup>-</sup>
NaOH·H <sub>2</sub> O	[Fe <sub>2</sub> (OH) <sub>2</sub> ] <sup>4+</sup>	[Fe(OH) <sub>4</sub> ] <sup>2-</sup>	[Fe(OH) <sub>4</sub> ] <sup>-</sup>
FeCl <sub>3</sub> ·6H <sub>2</sub> O	H <sup>+</sup>	[Fe(OH) <sub>3</sub> ] <sup>-</sup>	Na <sup>+</sup>

Table 2. Experimental parameters.

Sample	FeCl <sub>3</sub> ·6H <sub>2</sub> O(mol)	FeCl <sub>2</sub> ·4H <sub>2</sub> O(mol)	BOH(mol)	Final pH
S1	0.02	0.01	0.08 (NaOH)**	10.34
S2	0.02	0.01	0.085 (NaOH)	11.94
S3	0.02	0.01	0.09 (NaOH)	12.08
S4	0.02	0.01	0.095(NaOH)	12.20
S5	0.02	0.01	0.1(NaOH)	12.60
F1 <sub>Na</sub>	0.02	0.01	0.08 (NaOH)**	9.4
F3 <sub>Na</sub>	0.02	0.01	0.09 (NaOH)	10.7
F5 <sub>Na</sub>	0.02	0.01	0.1 (NaOH)	11.8
F3 <sub>K</sub>	0.02	0.01	0.09 (KOH)	-
F3 <sub>TEA</sub>	0.02	0.01	0.09(TEAOH)	-
*F3 <sub>TEA</sub>	0.02	0.01	0.09(TEAOH)	-

\*fast and reverse addition of solution containing ferric and ferrous ions into the TEAOH-containing solution; \*\*stoichiometric amount of base.

Table 3. Properties of magnetite samples.

Sample	Size (nm)		Specific surface area (m <sup>2</sup> /g)		Interface area (m <sup>2</sup> /g)	Ms(emu/g)
	XRD	BET	XRD	BET	(S <sub>XRD</sub> -S <sub>BET</sub> )/2	
S1	11.5	12.9	100.7	89.4	5.6	75.3
S2	11.2	12.4	103.4	93.3	5.1	71.6
S3	11.0	12.0	105.3	97.1	4.1	69.8
S4	10.9	11.8	106.3	97.8	3.5	69.4
S5	10.7	11.6	108.3	99.4	4.5	68.3
F1 <sub>Na</sub>	10.2	11.8	113.6	98.1	7.7	64.8
F3 <sub>Na</sub>	9.1	10.0	127	109	9.0	58.1
F5 <sub>Na</sub>	8.2	8.9	141.3	130.0	5.6	54.1
F3 <sub>K</sub>	7.1	7.6	163.1	152.4	5.3	53.6
F3 <sub>TEA</sub>	6.5	6.9	178.2	167.9	5.1	52.3
*F3 <sub>TEA</sub>	6.4	6.5	180.8	178.3	1.2	52.2

\*fast and reverse addition of solution containing ferric and ferrous ions into the TEAOH-containing solution.

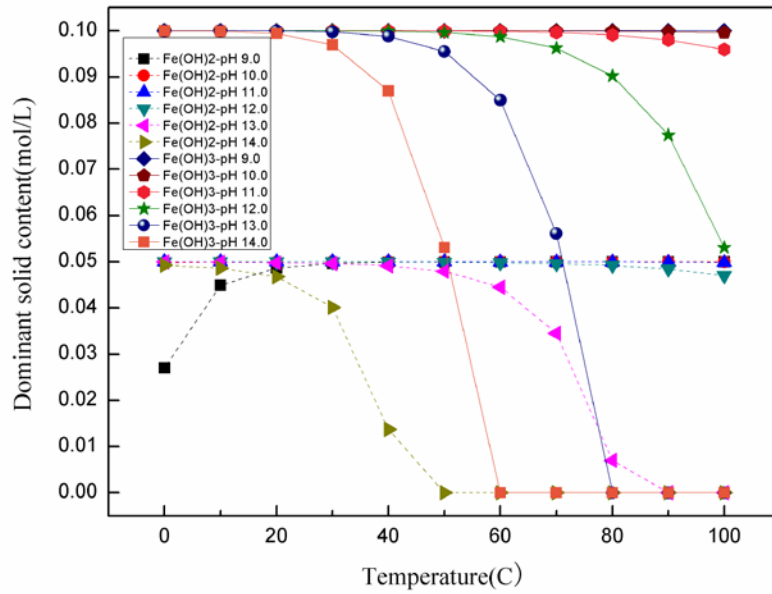


Figure 1(a). Dominant Solids ( $\text{Fe}(\text{OH})_2$  and  $\text{Fe}(\text{OH})_3$ ) concentration [mol/L] as a function of temperature at various pH values. Other solids are not precipitated at these conditions.

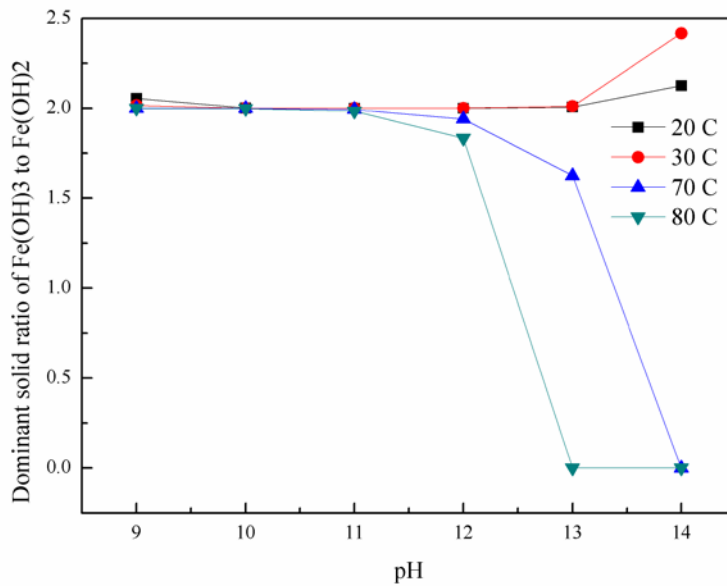
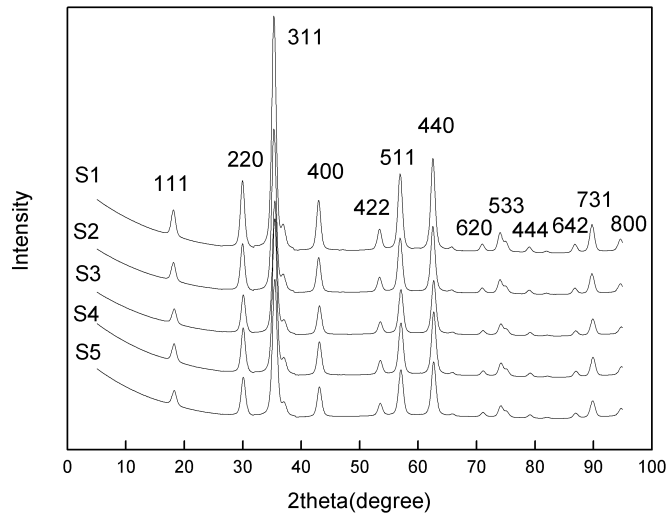
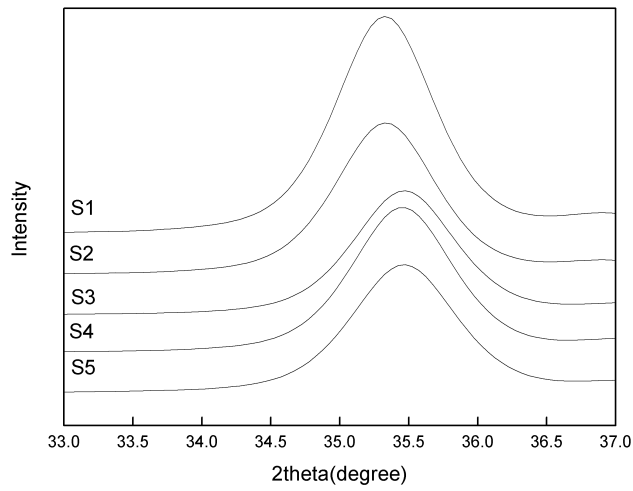


Figure 1(b). Dominant solids ratio of  $\text{Fe}(\text{OH})_3$  to  $\text{Fe}(\text{OH})_2$  at room temperature (20-30 °C) and high temperature (70-80 °C) at various pH values.



**Figure 2.** X-ray diffraction of magnetite nanoparticles synthesized at various NaOH amounts.



**Figure 3.** [3 1 1] peaks of the magnetite nanoparticles in expanded 2θ scale.

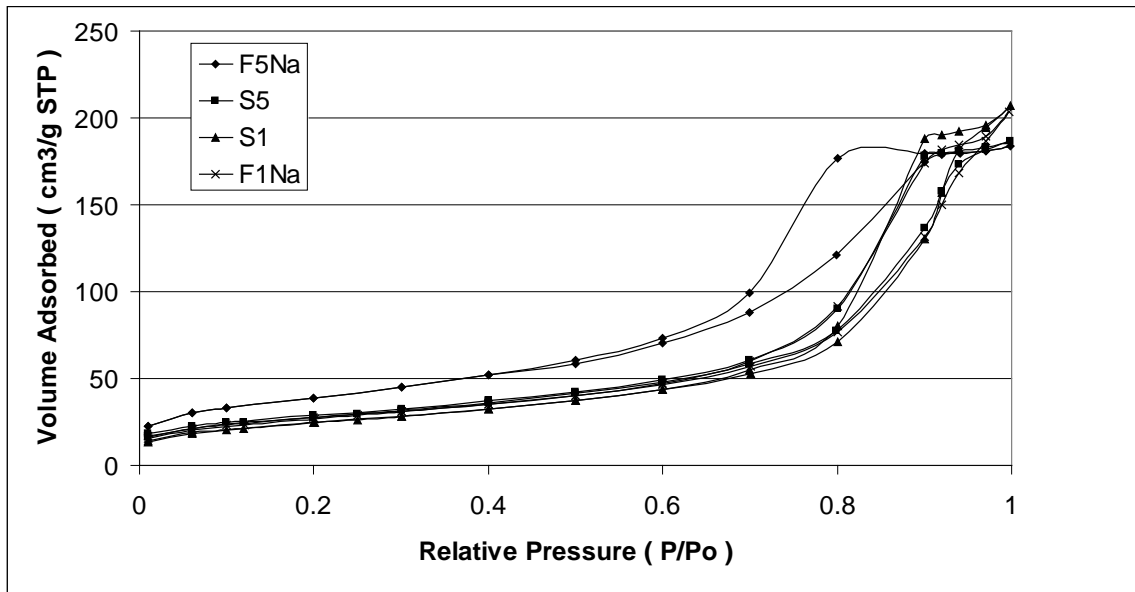


**Figure 4.** N<sub>2</sub> adsorption-desorption isotherms of S1, S5, F1<sub>Na</sub> and F5<sub>Na</sub> samples.

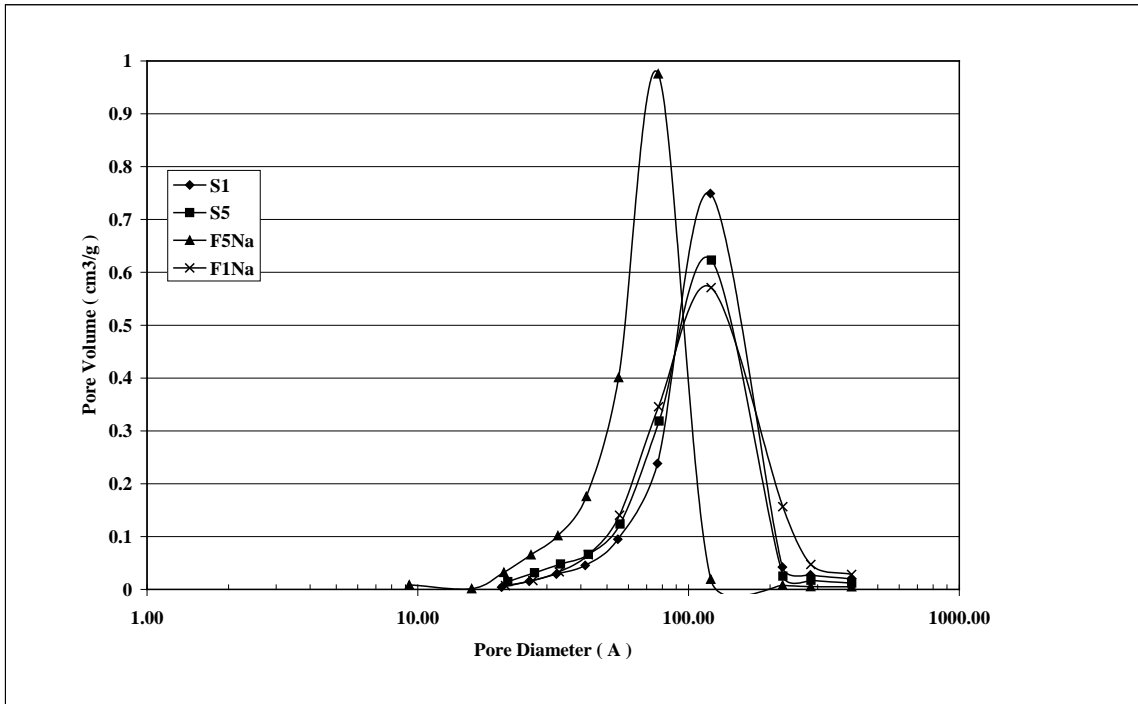


**Figure 5.** BJH desorption pore size distribution curves for S1, S5, F1<sub>Na</sub> and F5<sub>Na</sub> samples

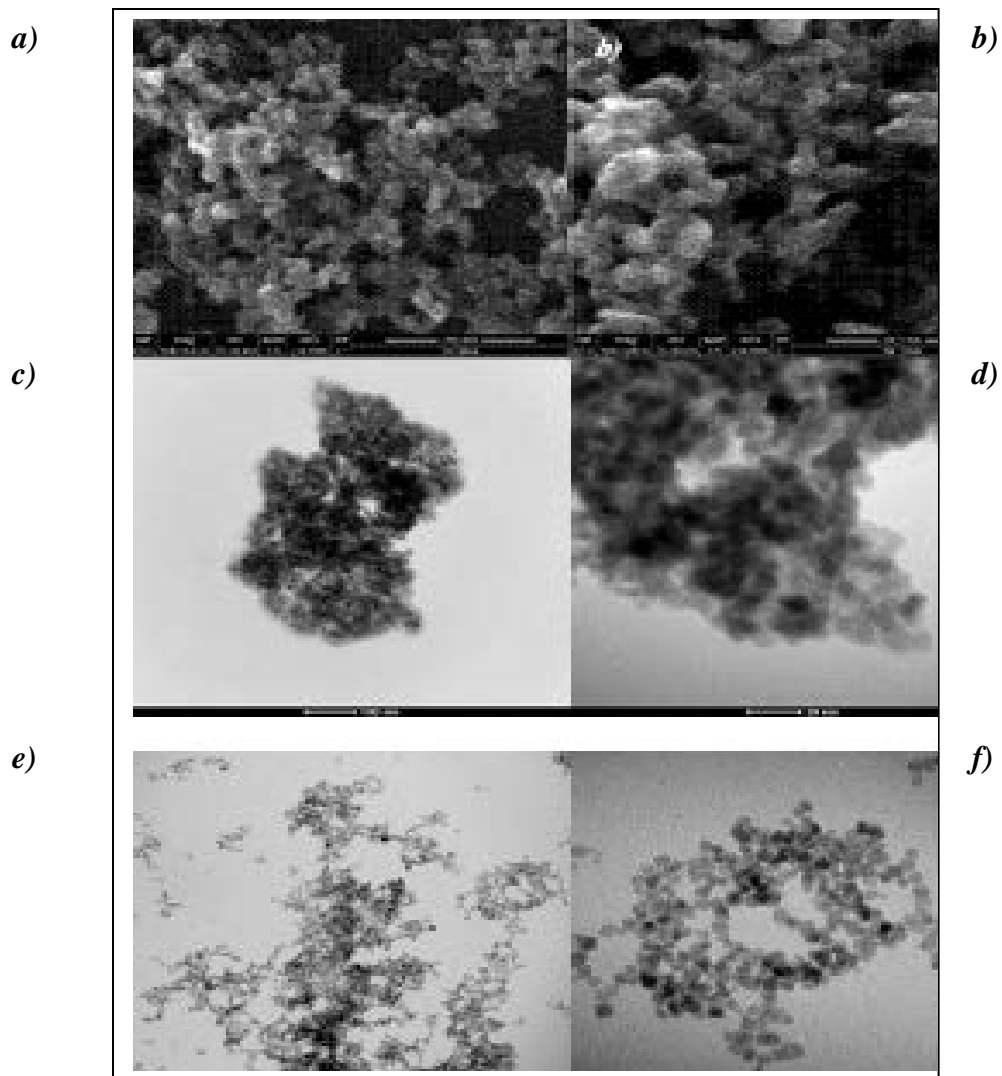


Figure 6. SEM images of S4 (a), S5 (b) samples and TEM images of F3<sub>Na</sub> (c, d), \*F3<sub>TEA</sub> (e, f).

**Figure7** Magnetization curves for S1, S2, F1Na and F5Na samples

